Kelvin waves in stratospheric temperature observed by the Microwave Limb Sounder

Philip W. Mote and Timothy J. Dunkerton
Northwest Research Associates, Bellevue, Washington

Dong Wu
Jet Propulsion Laboratory, Pasadena, California

Short title: KELVIN WAVES IN STRATOSPHERIC TEMPERATURE

Abstract. The three-dimensional structure of stratospheric Kelvin waves is revealed using data from the Microwave Limb Sounder (MLS) for the period July 1992–April 1993. Four Kelvin wave modes are identified, two for zonal wavenumber one ($k = 1$) and two for $k = 2$, using extended empirical orthogonal functions. The 3-D structures of the modes agree with linear theory and satisfy the dispersion relation for Kelvin waves, and with periods ranging from 4.5 days to 10 days, the modes mostly fall near the boundary between "fast" and "slow" Kelvin waves [*Canziani et al.* 1998]. The analysis also identifies a feature that may correspond with the "pancake structures" associated with inertial instability.

1. Introduction

On time scales less than 90 days, the dominant eastward-propagating features in the tropical stratosphere are produced by atmospheric Kelvin waves [e.g., *Wallace and Kousky*, 1968]. Kelvin waves, which are equatorially trapped, perturb the temperature, zonal wind, and trace constituent fields. *Tsuda et al.* [1994], *Fujiwara et al.* [1998], and *Boehm and Verlinde* [2000] showed that Kelvin waves influence tropopause structure and upper tropospheric cirrus clouds, giving them an important role in stratosphere-troposphere exchange and the radiative properties of the upper troposphere. Indeed, the sharp cooling of the tropopause that is sometimes associated with Kelvin waves [e.g., *Boehm and Verlinde*, 2000] may be an important missing factor in the attempt to explain the observed water vapor mixing ratios in the stratosphere, which are generally thought to be lower than one would expect from considering time-mean tropical tropopause temperatures.

Observations from satellite-based instruments have shown the structure of Kelvin waves in temperature (e.g., *Hirota* [1979, *Canziani et al.* [1994] and *Canziani and Holton* [1998]), and in trace constituents (e.g., *Randel* [1990], *Kawamoto et al.* [1997]). In this study, we extend the earlier study by *Canziani et al.* [1994], which used an earlier version of MLS data, in which temperature was available only at and above the 22-hPa MLS level. The present study extends theirs in period of record (288 days instead of two shorter periods of 70 days and 65 days), vertical extent (down to 68 hPa), and analysis techniques. Whereas they presented slices of data in various combinations of space and time, and analyzed power spectra and the coherence between temperature and ozone variations, the present study uses more statistical tools to extract coherent patterns in order to study the the structure of Kelvin waves in longitude, latitude, and height, and compares the structure with properties expected from linear theory. This work serves as a foundation for considering in a subsequent paper whether the variations in lower stratospheric water vapor noted by *Mote et al.* [1998a] can be linked with Kelvin waves.

The technique used here to identify coherent patterns in the data is called extended empirical orthogonal functions (EEOFs). A form of principal components analysis, EEOFs are useful for extracting coherent spatio-temporal variations, and have been used in a number of studies. *Weare and Nasstrom* [1982] introduced the technique and illustrated its use on monthly mean 300 hPa relative vorticity and on tropical Pacific sea surface temperature. It has also been used in studies of the stratospheric quasi-biennial oscillation [*Wang et al.,* 1995], regional [*Fraedrich et al.,* 1997] and global [*Clark et al.,* 1998] tropical tropospheric disturbances, and annual variations of stratospheric water vapor [*Mote et al.,* 1998b]. *Mote et al.* [2000] introduced multivariate EEOFs in a study of the tropical intraseasonal oscillation.

2. Data

The Microwave Limb Sounder (MLS) on the Upper Atmosphere Research Satellite (UARS) measures atmospheric radiation in a number of spectral bands. Temperature is retrieved using the 63 GHz band. The data are retrieved on a grid with 6 levels per factor of 10 in pressure, i.e., 68.1 hPa, 46.4, 31.6, 21.5, 14.7, 10, 6.81, and so on, with a vertical spacing of approximately 2.7 km. Version 5 (V5) data are used [*Livesey et al.*, 2001].

For this study we focus on the tropics, i.e., latitudes between 27.5°S and 27.5°N. The profiles of temperature observed by MLS are first averaged using bins of width 24° longitude and 5° latitude for each day. While the longitudinal resolution may seem very coarse, it is ample for resolving the features of interest, which tend to have most of their power in zonal wavenumbers 1 and 2. Tests with higher longitudinal resolution indicated that the resolution does not affect the results. On most days there are over 500 profiles within this latitude band (out of a global total of over 1300 per day), and consequently the typical bin contains about three profiles. Since we are focusing on time scales longer than $\sim$4 days and on a phenomenon with essentially no diurnal dependence, the results

should be insensitive to the fact that we have ignored the time of observation in forming these binned averages.

The MLS V5 algorithm retrieves temperatures above the 68 hPa pressure level on every UARS surface, but the range of reliable temperatures is 32 – 0.46 hPa. At altitudes below 32 hPa, MLS temperature sensitivity reduces sharply and the output temperatures are constrained to values from the reanalyses produced by the National Centers for Environmental Prediction (NCEP). At 46 hPa the output temperature includes about a 70% contribution from MLS, as estimated based on the error reduction to the a priori uncertainty in the retrieval, but at 68 hPa the contribution from MLS is less than 5%. The features identified here in MLS data were not evident in NCEP reanalysis data, nor in similar gridded data produced by the UK Meteorological Office, probably because there are too few actual soundings in the tropics to constrain the data assimilation models to produce these tropical waves.

The UARS, launched in September 1991, experienced technical problems in June and early July of 1992, and we use a period of record from July 10, 1992 to April 23, 1993 (UARS days 303 to 590, 288 days). This period of record was chosen partly for efficiency of the fast Fourier transform, partly because it is one of the longest nearly continuous periods in the MLS data, and partly to match the availability of water vapor data for a subsequent study. The data are high-pass filtered to retain only periods less than 90 days, and small gaps (all but two of which are only one day long) are filled by interpolation in time.

3. Identification of modes

Kelvin waves are equatorially trapped modes with strongest amplitude on the equator. Wavenumbers 1 and 2 predominate; following *Canziani and Holton* [1998], for some of the analysis shown below, we reduce the longitudinal structure of temperature variations at the equator to a single value by taking the component of the temperature

field that projects onto the cosine of longitude (Figure 1). Downward-propagating features frequently appear, and are especially deep and coherent in September 1992 and February 1993. The same can be done for the sine component, and the results are not significantly different. Figure 1

Further characteristics of the equatorial temperature data are revealed in plots of spectral power against wavenumber and frequency (Figure 2a). Wavenumber 1 dominates both eastward and westward waves. Although some spectral power is found in the intraseasonal frequency band (periods between 20 and 90 days), most power is found between 5 and 11 days, with the greatest power at 9.7 days for eastward wavenumber 1 ($k = 1$). Total power at the equator is roughly one-third as much for $k = 2$ as for $k = 1$. That the spectral peak at 9.7 days dominates throughout the tropical stratosphere is apparent from Figure 2b, which displays spectral power for $k = 1$ against frequency and pressure (top panel) and against frequency and latitude (bottom panel). The 9.7 day spectral peak is marked with a line in each panel. Spectral power is concentrated in the upper stratosphere and near the equator. These features are consistent with our interpretation that the dominant variations seen in Figure 1 are associated with stratospheric Kelvin waves. Similar figures (Figure 3) for $k = 2$ show dominant spectral peaks near 4.5 and 6 days, with very little power in the lower stratosphere but with similar confinement near the equator. Figure 2 Figure 3

In order to elucidate the relationships among variations at different levels, we perform extended empirical orthogonal function (EEOF) analysis on the data presented in Figure 1. We use a window of ± 10 days and a time step of 2 days; the results are not very sensitive to the choices of window and time step. The EEOF analysis (Figure 4) isolates three distinct downward-propagating patterns, each with different structure and propagation characteristics. Each type is characterized by a conjugate pair of very similar EEOFs. It is generally true for EOFs (including EEOFs) that the characteristic features of conjugate pairs of EOFs include (1) very similar structure, but shifted Figure 4

one-quarter cycle; (2) principal component time series in quadrature; (3) nearly equal eigenvalues for the two members of the pair. Such behavior is typical of a propagating phenomenon [e.g., *Weare and Nasstrom,* 1982; *Mote et al.,* 1998a].

The first pair of EEOFs together represent 22% of the variance, and describe a variation whose period is 10 days (estimated by averaging the peak-to-peak interval at various levels in Figure 4) and whose vertical wavelength increases from about 14 km in the lower stratosphere to about 20 km in the upper stratosphere. Their vertical phase speed changes from -1.1 cm s^{-1} in the lower stratosphere to -3.1 cm s^{-1} in the upper stratosphere, resulting in a somewhat curved shape of the phase lines. The second pair of EEOFs together represent 13% of the variance and describe a variation whose period is about 6.5 days and whose vertical wavelength is about 23 km, though the variations are so weak in the lower stratosphere that it is difficult to estimate the wavelength. The vertical phase speed is about -4.1 cm s^{-1}. The third pair of EEOFs explains 11% of the variance and, like the second, has considerably less power in the lower stratosphere. The variation described by this pair has a period around 17 days, a vertical wavelength of about 19 km in the upper stratosphere, and a vertical phase speed of -1.5 cm s^{-1}. The first three pairs of EEOFs, which together explain about half (46%) of the variance, correspond roughly with the spectral peaks at around 9–10, 6–7, and 14–18 days shown in Figure 2b. The higher-order EEOFs (not shown) have irregular structures and do not appear to be distinct, physically meaningful modes.

Similar results are obtained when the EEOFs are calculated after processing the data in other ways. For example, the leading EEOFs and their eigenvalues are similar if calculated from the projection of the temperature field onto the sine component instead of the cosine component, or when the altitude range or the period of record used in the calculation is changed somewhat. Consequently, we believe that these patterns are robust features of the MLS temperature data over this time period.

Associated with each EEOF is a principal component time series (PC); these are

plotted in Figure 5. PCs 1 and 2 are very regular and nearly periodic (with a sharp spectral peak, not shown, at 9.8 days), and are in quadrature as expected. Their amplitudes are large in late August and early September 1992, and in January and February 1993, corresponding to periods of large wave activity visible in Figure 1. When the time series of PC1 and PC2 are plotted against each other (not shown, but see Figure 3c of *Mote et al.* [1998a] for an example), the traces are nearly circular orbits, yet another indication that these represent a wave-like phenomenon. Note the similarities among the period shown in Figure 2, the period estimated from the EEOFs, and the period estimated from the spectra of the PCs.

Figure 5

For the next pair of EEOFs (3 and 4), the time series are also very regular and nearly periodic, with a sharp spectral peak at 5.8 days, largest values around the end of December 1992, and fairly large values for about the last three-fifths of the period of record. Spectral power near this peak can be seen in Figure 2, and it is concentrated in the upper stratosphere, consistent with the structure of EEOFs 3 and 4 shown in Figure 4.

By contrast with the first two pairs of PCs, the third pair of PC's behaves somewhat irregularly and the two time series are not clearly in quadrature. The spectra of these two PCs are very broad, with a peak at about 16 days and a smaller peak at about 5.7 days.

Repeating the EEOF calculation for $k = 2$ variations, we again find leading modes that represent a downward-propagating variation (Figure 6). The first pair of EEOFs has a characteristic timescale of 4.5 days and explains 18% of the variance, the second pair has a timescale of 6 days and explains 15% of the variance, and the third pair has a timescale of about 11 days and explains 11% of the variance. These first three modes explain less variance than the first three modes for $k = 1$.

Figure 6

For $k = 1$ we used a time interval of two days in the EEOF calculation, but for $k = 2$ we use a time interval of one day in order to present the variations more clearly.

The EEOFs themselves are essentially the same with a two-day interval, but are shown less clearly. The second pair of EEOFs bears a striking resemblance to the second pair calculated from the $k = 1$ projection of the temperature data, an observation that has interesting consequences, as we shall see shortly.

We now check whether these temperature variations satisfy the dispersion relation for Kelvin waves,

$$\omega - k\bar{u} = -Nk/m \tag{1}$$

where $\omega = 2\pi/\tau$, τ is the period, k and m are the zonal and vertical wavenumber respectively, and N is the Brunt-Väisälä frequency [e.g., *Andrews et al.,* 1987]. During the period of record used in this study, the zonal mean zonal wind $\bar{u}$ had a mean value between 10°S and 10°N of -8.7 ms^{-1}, or -12.0 ms^{-1} in the upper stratosphere (10-1 hPa) and -5.4 ms^{-1} in the lower stratosphere (100-10 hPa) (using UKMO data; *Swinbank and O'Neill*, 1994). For typical values of ω, k, and $\bar{u}$, $|\omega| >> |k\bar{u}|$ so the variation of $\bar{u}$ in time and space makes only a small difference. Using the values for m and τ mentioned above, we calculate (and round to the nearest integer) the LHS and RHS of (1); see Table 1. The first two modes, for both $k = 1$ and $k = 2$, satisfy the dispersion relation for Kelvin waves, but the third does not.

4. Spatial structure of Kelvin waves

In order to examine the spatial structure of these features and to add further evidence concerning whether they are Kelvin waves, we perform a regression analysis of the temperature data $T(x, y, z, t)$ against a reference time series e^i_{ref} for some of the patterns identified by EEOF analysis, yielding a set of spatial structures $T_i(x, y, z)$, one for each reference time series e^i. The reference time series consist of the first, third, and fifth PC of EEOFs for $k = 1$ (which were shown in Figure 5) and likewise for $k = 2$ (not shown). The EEOFs were calculated using data along the equator and between 46 and

0.68 hPa, but the reference time series are regressed against binned temperature data between 25°S and 25°N, and at levels from 68 to 0.22 hPa in order to extend the spatial domain. Recall that the MLS V5 retrieval provides reliable temperature data between 32 and 0.46 hPa. The 68, 46, and 0.22 hPa levels are included in order to search for coherence between variations at those levels and variations at the more reliable levels.

The results of this regression analysis are shown in Figure 7, in which the left-hand panels show longitude-altitude sections and the right-hand panels show latitude-altitude sections. All three of the patterns identified with EEOF analysis exhibit the characteristic phase tilt (upward and eastward) of Kelvin waves. However, on closer inspection there are several important differences between the third mode and a Kelvin wave. While the first and second pattern are equatorially trapped (maximum amplitude near the equator, decreasing away from the equator), the third is not. The zonal structure of the third pattern is a sharp peak near 0° rather than strongly wave-1.

Figure 7

The same analysis is repeated for the EEOFs for $k = 2$ (which were shown in Figure 6), and the result shown in Figure 8. The first two patterns have the characteristic upward and eastward phase tilt and they also have maximum amplitude near the equator, at least in the upper stratosphere and mesosphere. The sinusoidal wavenumber-2 structure is evident in the left-hand panel only for the first mode: the second pattern has $k = 1$ structure even though it was formed by regression using a time series derived from $k = 2$ variations. This is the interesting consequence of the similarity between EEOF3 for $k = 1$ and EEOF3 for $k = 2$ mentioned earlier. The $k = 1$ structure found here may reflect in part the low variance explained by this mode and its strong similarity to the second mode for $k = 1$, whose variance is much larger. Unlike all the other EEOFs shown here, the spatial structure of the third $k = 2$ EEOF (Figure 6) changes substantially with lag and altitude: the period increases from about 9 days in the upper stratosphere to about 13 days in the lower stratosphere, and the vertical phase speed decreases from about 3.7 to 2.6 cm s^{-1}. Because of this nonstationary behavior,

Figure 8

the quantites shown in Table I cannot be calculated for this mode. From Figure 8 it is apparent that the variance represented by this EEOF is very different from Kelvin waves.

The meridional structure of the variations shown in Figure 7 can be compared with the expected Gaussian profile (e.g., *Andrews et al.*, 1987) of equatorially trapped Kelvin waves. One way of quantifying the meridional structure was used by *Salby et al.* [1984] and *Canziani et al.* [1994]: the distance between the north and south quarter-power points. Here we develop a more elaborate method of examining the meridional structure, a method derived from linear theory. At each level, we first form the equatorially symmetric component of the regression data (we used correlations with similar results), then normalize and average the variations at those longitudes where the equatorial perturbation is at least 0.15K. Then this average $f(\phi)$ (ϕ representing latitude) is transformed using $\sqrt{-\log f(\phi)}$ and a linear fit is found (with a latitude-dependent weighting to favor latitudes nearer the equator); when transformed back, this gives a best-fit Gaussian. An example is shown in Figure 9 for 32 hPa. This procedure results in a fairly close fit to the observed structure at most levels, and highlights levels where the structure is non-Gaussian. The meridional length scale of interest is L_ϕ, the distance from the equator at which the line passes $\sqrt{-\log f(\phi)} = 1$. (Distances are converted here to latitude for clarity.) Values of L_ϕ thus derived are about 16° at 46 hPa, 18–19° at 32, 22, and 15 hPa, increasing to 20° at 10 hPa and 22° at 6.8 hPa. Other meridional weights, including constant and linearly decreasing functions of latitude, only changed these estimates of L_ϕ by between 0 and 3°. Above 6.8 hPa the structure no longer resembles a Gaussian curve. The average value of L_ϕ calculated by averaging the values at all the levels 46–6.8 hPa with all the different meridional weights is $2\overline{0}°$.

Figure 9

The meridional length scale expected on the basis of linear theory [easily derived from equations in, e.g., *Andrews et al.,* 1987, p. 203] is

$$L_\phi = |a\hat{c}/\Omega|^{1/2} \tag{2}$$

where a and Ω are the radius and angular velocity of the Earth, and $\hat{c} = c_x - \bar{u}$. Using $c = 48$ m s^{-1} and $\bar{u} = -8.7$ m s^{-1}, we obtain L_ϕ=20°, the same as the value estimated graphically above. Values of L_ϕ are estimated for the other modes and summarized in Table 1.

The same analysis is repeated for other EEOFs. For EEOF 3, the phase speed is 71 m s^{-1} and a more appropriate threshold for the equatorial perturbation is 0.075 K; we again find good agreement between L_ϕ estimated graphically (22°) and L_ϕ calculated from the equation above (24°). The values of L_ϕ decrease from 21° –25° at 46 and 32 hPa to 14° – 18° at 22 and 15 hPa, then increase again to about 19° at 6.8 and 25° at 4.6 hPa and stop resembling a Gaussian above that. For EEOF 5, the meridional structure does not resemble a Gaussian except in the lowest few levels of the mesosphere; note the hemispheric asymmetry, especially in the upper stratosphere (Figure 7, lower right panel). Consequently, this procedure fails to yield an estimate of L_ϕ, although using equation (1) yields a value of 16°. For the first EEOF of $k = 2$, L_ϕ estimated graphically is about 14° at most levels between 68 and 3 hPa, but the value calculated using equation (1) is 21°. For the second EEOF of $k = 2$, there is closer agreement between the two methods of estimating L_ϕ in the upper stratosphere; variations in the lower stratosphere associated with this mode are too weak to derive L_ϕ.

5. Summary and Conclusions

Equatorially trapped stratospheric Kelvin waves have previously been identified in both radiosonde data [e.g., *Tsuda et al.*, 1994] and satellite data [e.g., *Canziani et al.*, 1994]. However, because of its global coverage and high quality, the MLS Version 5 dataset affords a systematic look at the structure of Kelvin waves. Using EEOF analysis instead of the more common narrow spectral filtering, we have objectively identified the leading modes of wavenumber-1 and -2 variability in equatorial temperatures. When these modes are regressed on temperature observations in the stratosphere and lower

mesosphere, the structure of the first two distinct modes is consistent with linear Kelvin wave theory.

Previous work (as summarized by *Canziani et al.* [1994]) has found three discrete temporal bands for Kelvin waves: slow (with phase speeds of 20–40 ms^{-1} and vertical wavelength $\sim$ 10 km), fast (50–80 ms^{-1}, $\sim$ 20 km), and ultrafast ($\sim$ 80ms^{-1}, $\sim$ 40 km). The phase speed (48 ms^{-1}) and vertical wavelength (14–20 km) of the first mode identified in this paper lie roughly at the boundary between slow and fast Kelvin waves. The phase speed (71 ms^{-1}) and vertical wavelength (23 km) of the second mode falls under the category of fast Kelvin waves. Together, these first two modes represent 35% of the variance in wavenumber one.

For $k = 2$, the first mode has phase speed (51 m s^{-1}) and vertical wavelength (18 km) that places it, like the first mode of $k = 1$, roughly between slow and fast waves. Spectral power is so much larger for $k = 1$ than for $k = 2$ that regression of stratospheric temperatures on the principal component time series associated with the second $k = 2$ mode yields a surprising result: a meridional structure in which $k = 1$ predominates. The usual approach to Kelvin waves is to apply a spectral filter, which may overemphasize the degree of separation between modes of different wavenumber. Here, when we let the data speak for themselves by performing regression, we find that the second $k = 2$ mode is in some sense degenerate.

The third mode for $k = 1$ identified here does not satisfy the dispersion relation of the Kelvin wave, but may correspond to the "pancake structures" near the stratopause that are associated with inertial instability. Evidence in favor of this interpretation includes previous analysis of this same time period. *Hayashi et al.* [1998] noted the presence of such structures during the time period studied here, and they focused on features in early August 1992 and December 1992, when the amplitudes of PC5 and 6 are large (Figure 5). Amplitudes of PC5 and 6 are also large at other times (like September 1992 and January 1993) when a vertical dipole appears near the stratopause,

as shown in their version of our Figure 1. Other features of these modes that suggest a similarity to the pancake structures are the large variance stretching toward the northern subtropics in the lower mesosphere and the narrow confinement in longitude, to $\sim 0^\circ$ (Figure 7). Evidence against the interpretation of these EEOFs 5 and 6 as pancake modes is the structure of EEOFs 5 and 6 (Figure 4), which strongly suggests downward propagation, a characteristic not shared by the pancake structures, which are usually stationary in the vertical. However, *Smith and Riese* [1999] suggested that an episode of inertial instability was linked with Kelvin wave activity in the lower stratosphere observed in November 1994, and the same may have occurred during the time period studied here.

During this time period, equatorial winds were predominantly easterly; it would be interesting to see how the Kelvin wave properties found here change during the westerly phase of the QBO. Although MLS measurements continued throughout the 1990s, they grew more sporadic as the UARS aged, and consequently it would be increasingly difficult to find Kelvin waves using either the techniques described here or the more conventional spectral analysis, both of which rely on having fairly continuous measurements.

Acknowledgments. We thank Bill Randel, Nathaniel Livesey, Joe Waters, Bob Harwood, and two anonymous reviewers for helpful suggestions. This work was supported by NASA contracts NAS1-99130 and NAS5-98078.

References

Boehm, M.T., and J. Verlinde, Stratospheric influence on upper tropospheric tropical cirrus, *Geophys. Res. Lett., 27,* 3209–3212, 2000.

Canziani, P.O., J.R. Holton, E. Fishbein, L. Froidevaux, and J.W. Waters, Equatorial Kelvin waves: a UARS MLS view, *J. Atmos. Sci., 51,* 3053–3076, 1994.

Canziani, P.O, and J.R. Holton, Kelvin waves and the quasi-biennial oscillation: An observational analysis, *J. Geophys. Res., 103*, 31,509–31,521, 1998.

Clark, H.L., R.S. Harwood, P.W. Mote, and W.G. Read, Variability of water vapor in the tropical upper troposphere as measured by the Microwave Limb Sounder on UARS, *J. Geophys. Res., 103*, 31,695–31,707, 1998.

Fujiwara, M., K. Kita, and T. Ogawa, Stratosphere-troposphere exchange of ozone associated with the equatorial Kelvin wave as observed with ozonesondes and radiosondes, *J. Geophys. Res., 103*, 19,173–19,182, 1998.

Hayashi, H., M. Shiotani, and J.C. Gille, Vertically stacked temperature disturbances near the equatorial stratopause as seen in cryogenic limb array etalon spectrometer data, *J. Geophys. Res., 103*, 19,469–19,483, 1998.

Hirota, I., Kelvin waves in the equatorial middle atmosphere observed with Nimbus 5 SCR, *J. Atmos. Sci. 36*, 217–222, 1979.

Kawamoto, N., M. Shiotani, and J.C. Gille, Equatorial Kelvin waves and corresponding tracer oscillations in the lower stratosphere as seen in LIMS data, *J. Meteorol. Soc. Japan, 75,* 763–773, 1997.

Livesey, N.J., W.G. Read, L. Froidevaux, J.W. Waters, H.C. Pumphrey, D.L. Wu, M.L. Santee, Z. Shippony, and T.A. Lungu, The UARS Microwave Limb Sounder version 5 dataset: Theory, characterization and validation. Manuscript in preparation, 2001.

Mote, P.W., T.J. Dunkerton, and H.C. Pumphrey, Sub-seasonal variations in lower stratospheric water vapor, *Geophys. Res. Lett., 25*, 2445–2448, 1998a.

Mote, P.W., T.J. Dunkerton, M.E. McIntyre, E.A. Ray, P.H. Haynes, and James M. Russell III, Vertical velocity, vertical diffusion, and dilution by midlatitude air in the tropical

lower stratosphere, *J. Geophys. Res., 103,* 8651–8666, 1998b.

Mote, P.W., H.L. Clark, T.J. Dunkerton, R.S. Harwood, and H.C. Pumphrey, Intraseasonal variations of water vapor in the tropical upper troposphere and tropopause region, *J. Geophys. Res., 105*, 17,457–17,470, 2000.

Randel, W.J., Kelvin wave-induced trace constituent oscillations in the equatorial stratosphere, *J. Geophys. Res., 95*, 18,641–18,652, 1990.

Salby, M.L., D.L. Hartmann, P.L. Bailey, and J.C. Gille, Evidence for equatorial Kelvin modes in Nimbus-7 LIMS, *J. Atmos. Sci. 41*, 220–235, 1984.

Smith, A.K., and M. Riese, Cryogenic Infrared Spectrometers and Telescopes for the Atmosphere (CRISTA) observations of tracer transport by intertially unstable circulations *J. Geophys. Res., 104*, 19,171–19,182, 1999.

Swinbank, R.S., and A. O'Neill, A stratosphere-troposphere data assimilation system, *Mon. Wea. Rev., 122,* 686–702, 1994.

Tsuda, T., Y. Murayama, H. Wiryosumarto, S.W.B. Harijono, and S. Kato, Radiosonde observations of equatorial atmospheric dynamics over Indonesia, 1. Equatorial waves and diurnal tides, *J. Geophys. Res., 99,* 10,491–10,505, 1994.

Wallace, J.M., and V.E. Kousky, Observational evidence of Kelvin waves in the tropical stratosphere, *J. Atmos. Sci., 25,* 900–907, 1968.

Weare, B.C., and J.S. Nasstrom, Examples of extended empirical orthogonal function analysis, *Mon. Wea. Rev., 110,* 481–485, 1982.

T.J. Dunkerton and P.W. Mote, Northwest Research Associates, PO Box 3027, Bellevue WA 98009. (mote@nwra.com, tim@nwra.com)

Dong Wu, Jet Propulsion Laboratory, 4800 Oak Grove Drive, Pasadena CA

Received August 2001; revised November 2001; accepted .

Table 1. Wave properties of leading EEOFs

mode	τ[a]	λ_z[a]	c_z[a]	c_x	L_ϕ[b]	L_ϕ[c]	$\omega - k\bar{u}$	$-Nk/m$
$k = 1$ EEOF1 US	10d	20 km	-3.1 cm s^{-1}	48 m s^{-1}	—	20°	9 s^{-1}	10 s^{-1}
" LS	10d	14 km	-1.1 cm s^{-1}	48 m s^{-1}	20°	20°	8 s^{-1}	8 s^{-1}
EEOF3	6.5d	23 km	-4.1 cm s^{-1}	71 m s^{-1}	22°	24°	13 s^{-1}	13 s^{-1}
EEOF5	17d	19 km	-1.5 cm s^{-1}	27 m s^{-1}	—	16°	6 s^{-1}	11 s^{-1}
$k = 2$ EEOF1	4.5d	18 km	-4.6 cm s^{-1}	51 m s^{-1}	14°	21°	19 s^{-1}	20 s^{-1}
EEOF3 US	6d	14 km	-3.2 cm s^{-1}	39 m s^{-1}	16°	18°	15 s^{-1}	16 s^{-1}

[a]Estimated graphically from Figure 4 or 6.

[b]Estimated graphically as in Figure 9.

[c]Estimated using equation (2).

LS: Lower stratosphere. US: upper stratosphere.

Figure 1. Time-height plot of the projection of equatorial temperature onto the cosine of longitude (wavenumber-one component). Tick marks on the x-axis are placed at the first day of the month indicated. Contour interval is 1K, and shading indicates negative values.

Figure 2. Power spectra of the MLS temperature data. (a) wavenumber-frequency spectra at the equator computed at each level between 68 and 0.68 hPa and then summed. Positive wavenumbers indicate eastward-traveling waves, and the power at wavenumber zero has been suppressed. Note the maximum at eastward wavenumber 1 and a period of 9.7 days. (b) Power spectra for eastward wavenumber 1 shown (top) at the equator as a function of pressure and frequency and (bottom) at 4.6 hPa as a function of latitude and frequency. The long line in each panel shows the intersection point with the other panel. The short line indicates the period at which maximum power occurs (9.7 days).

Figure 3. As in Figure 2b but for wavenumber 2.

Figure 4. Lag-altitude structure of first 6 EEOFs of the $k = 1$ cosine component of equatorial temperature. The first 6 EEOFs represent three conjugate pairs.

Figure 5. Principal component time series of the EEOFs shown in Figure 4.

Figure 6. As in Figure 4 but for $k = 2$.

Figure 7. Structure of temperature variations associated with the first, third, and fifth EEOFs shown in Figure 4. For each row, a three-dimensional temperature structure is formed by regressing the gridded (longitude-latitude-height) MLS V5 temperature data against the principal component time series shown in Figure 5. Left column shows longitude-altitude structure at the equator, and right column shows latitude-altitude structure at a longitude of 0°.

Figure 8. As in Figure 7 but for $k = 2$.

Figure 9. Meridional structure of the temperature variations shown in the top panels of Figure 7. The set of curves tending down from a value of 1 are the normalized components at different longitudes; the curve marked with diamonds is their average. The plain solid curve is the best-fit Gaussian structure derived as explained in the text. The two curves passing through the origin are the transformation of the two solid curves passing through 1, with the straight line being a linear fit (using the weights shown in the right-hand panel) to the curve marked with diamonds. The straight line has a value of 1.0 at latitude 18.5° ($=L_\phi$). Note how closely the Gaussian curve approximates the observed structure out to about 17° latitude.

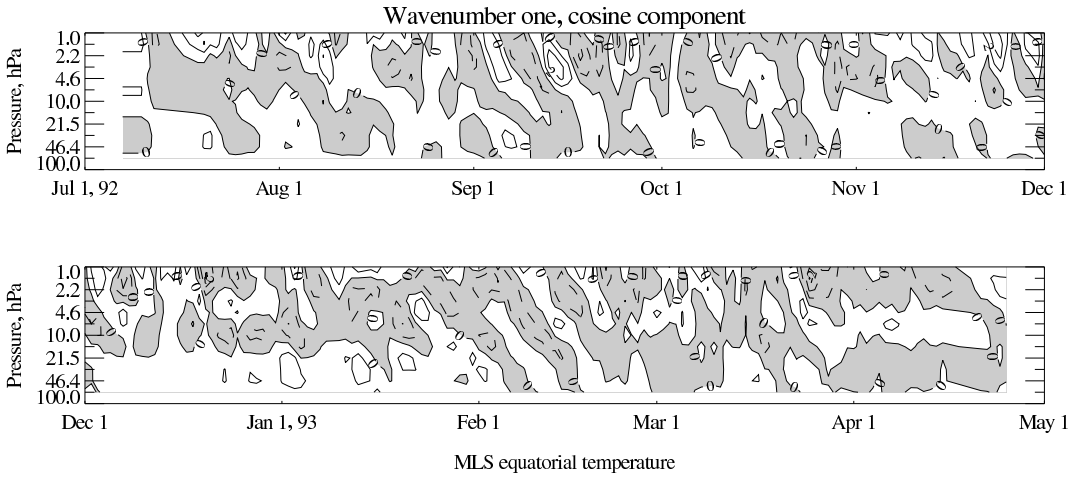

Figure 1: Time-height plot of the projection of equatorial temperature onto the cosine of longitude (wavenumber-one component). Tick marks on the x-axis are placed at the first day of the month indicated. Contour interval is 1K, and shading indicates negative values.

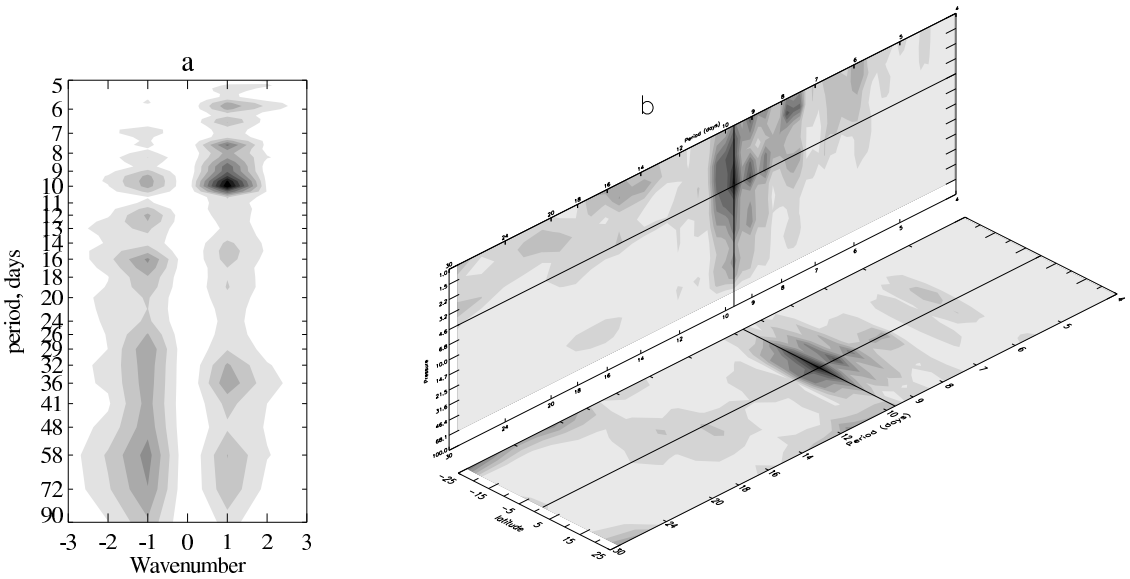

Figure 2: Power spectra of the MLS temperature data. (a) wavenumber-frequency spectra at the equator computed at each level between 68 and 0.68 hPa and then summed. Positive wavenumbers indicate eastward-traveling waves, and the power at wavenumber zero has been suppressed. Note the maximum at eastward wavenumber 1 and a period of 9.7 days. (b) Power spectra for eastward wavenumber 1 shown (top) at the equator as a function of pressure and frequency and (bottom) at 4.6 hPa as a function of latitude and frequency. The long line in each panel shows the intersection point with the other panel. The short line indicates the period at which maximum power occurs (9.7 days).

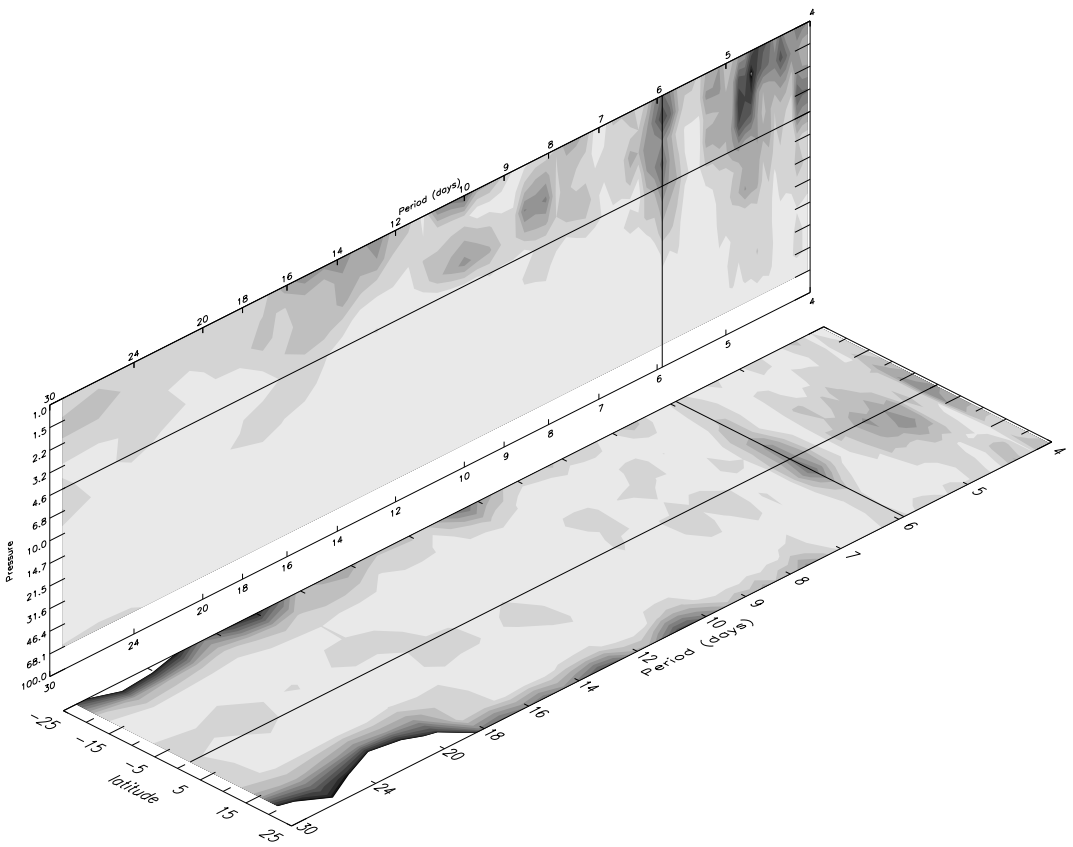

Figure 3: As in Figure 2b but for wavenumber 2.

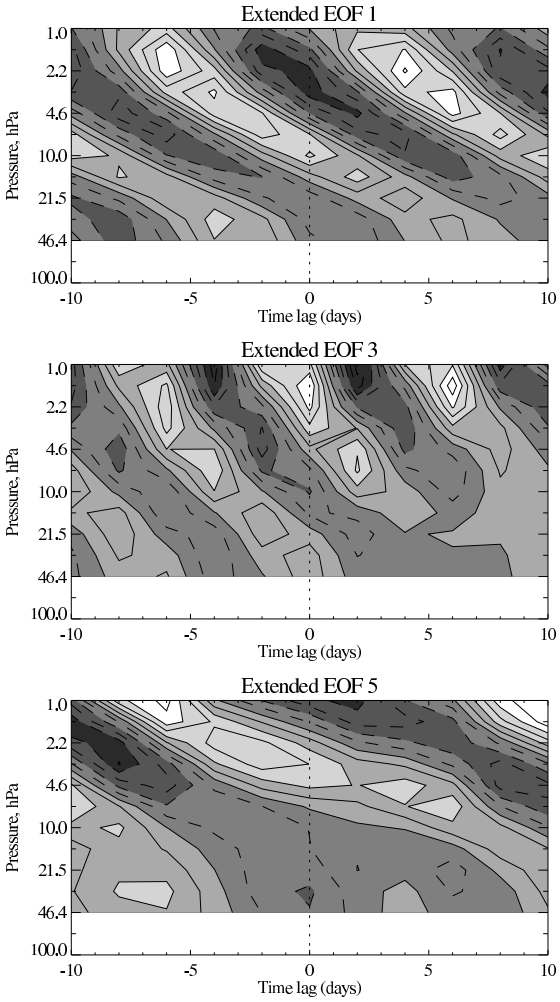

Figure 4: Lag-altitude structure of first 6 EEOFs of the $k = 1$ cosine component of equatorial temperature. The first 6 EEOFs represent three conjugate pairs.

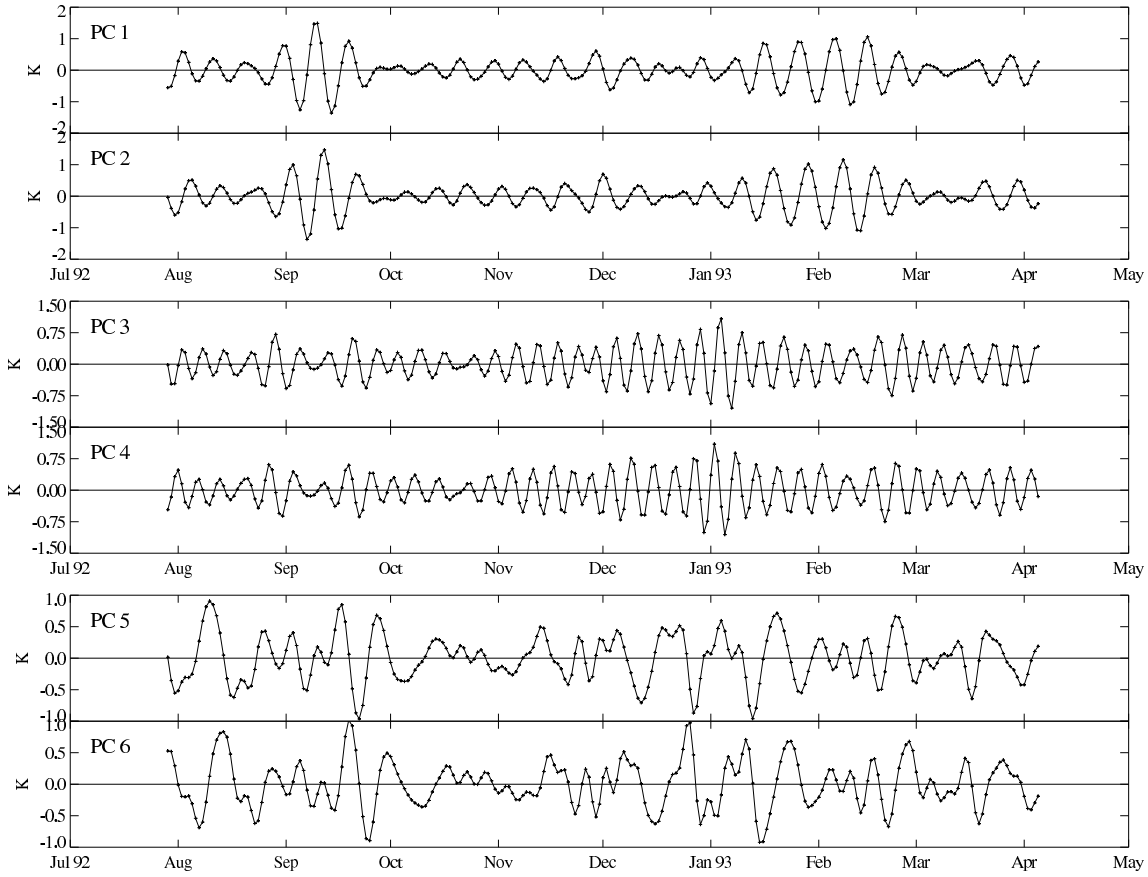

Figure 5: Principal component time series of the EEOFs shown in Figure 4.

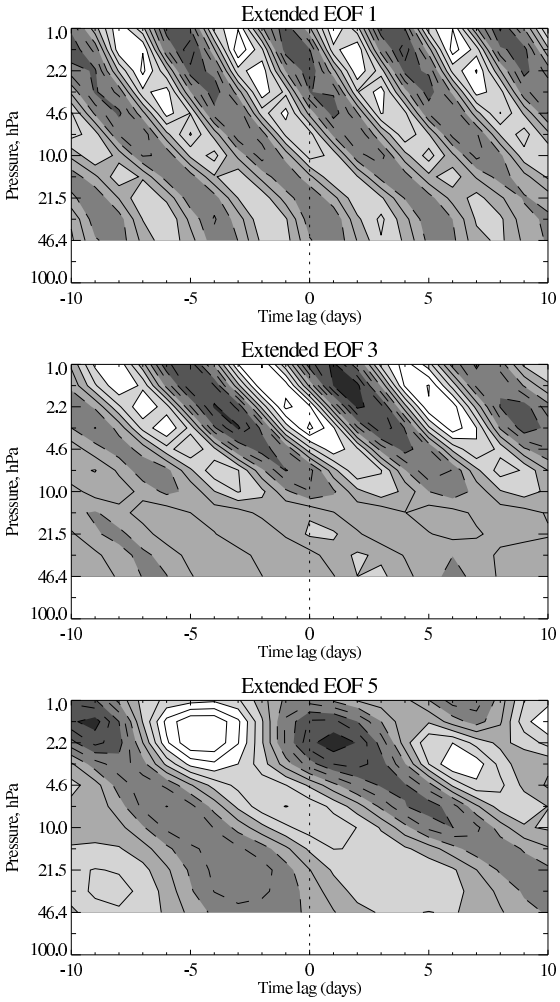

Figure 6: As in Figure 4 but for $k = 2$.

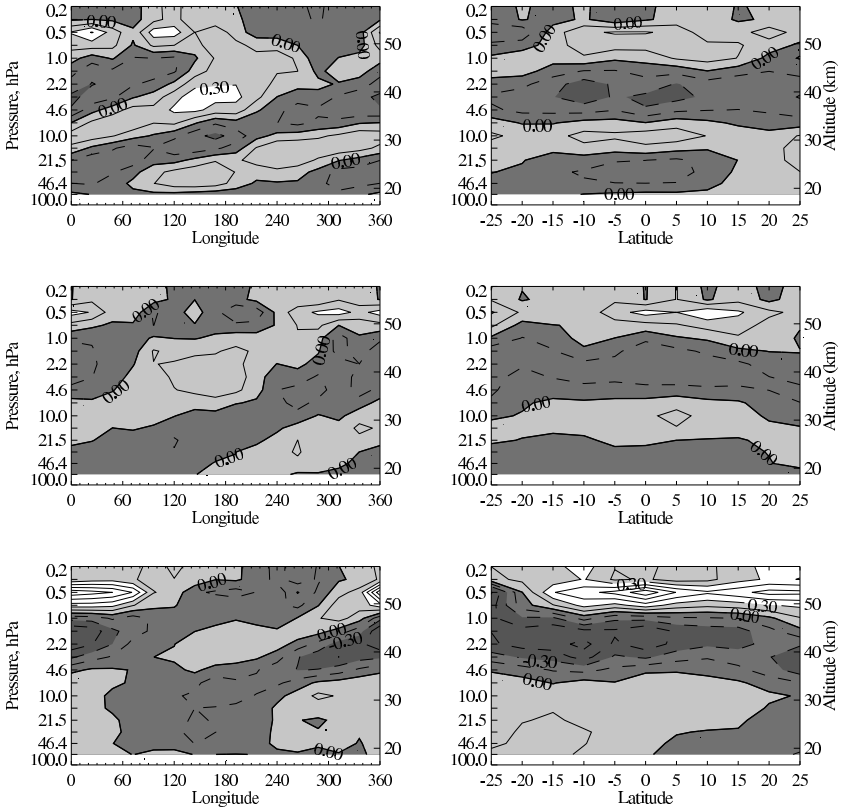

Figure 7: Structure of temperature variations associated with the first, third, and fifth EEOFs shown in Figure 4. For each row, a three-dimensional temperature structure is formed by regressing the gridded (longitude-latitude-height) MLS V5 temperature data against the principal component time series shown in Figure 5. Left column shows longitude-altitude structure at the equator, and right column shows latitude-altitude structure at a longitude of 0°.

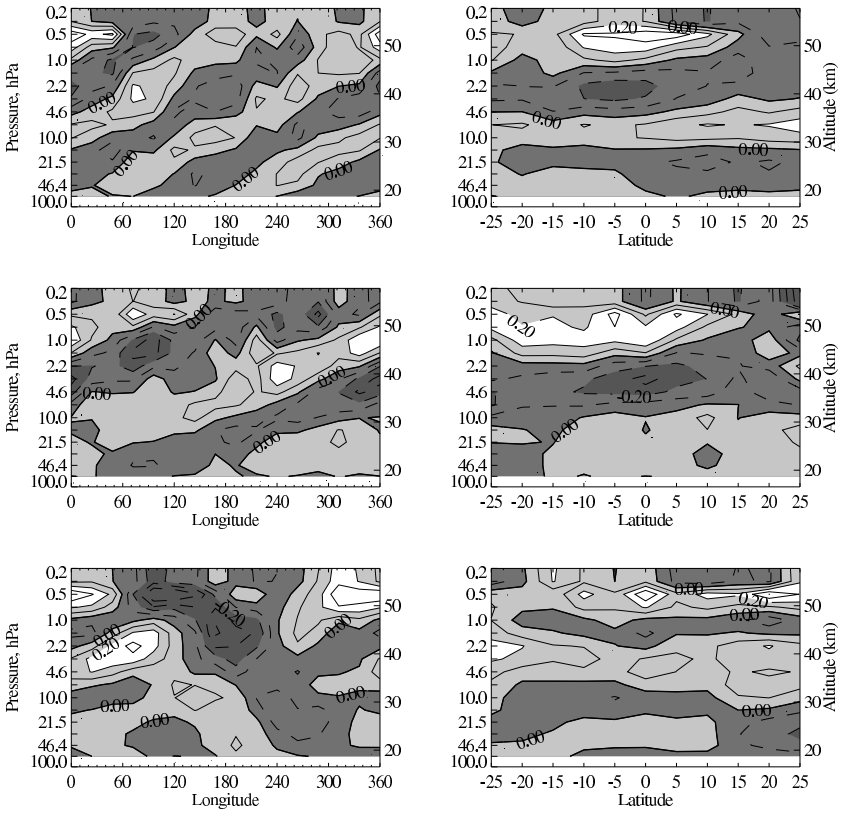

Figure 8: As in Figure 7 but for $k = 2$.

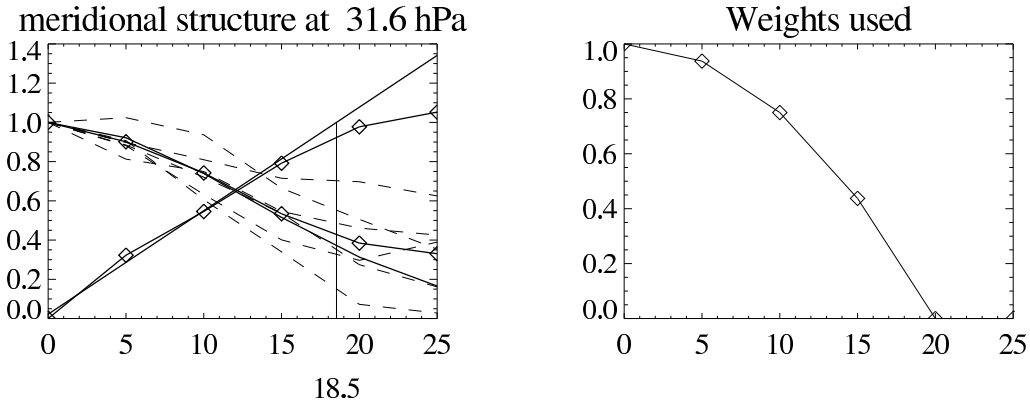

Figure 9: Meridional structure of the temperature variations shown in the top panels of Figure 7. The set of curves tending down from a value of 1 are the normalized components at different longitudes; the curve marked with diamonds is their average. The plain solid curve is the best-fit Gaussian structure derived as explained in the text. The two curves passing through the origin are the transformation of the two solid curves passing through 1, with the straight line being a linear fit (using the weights shown in the right-hand panel) to the curve marked with diamonds. The straight line has a value of 1.0 at latitude 18.5° ($=L_\phi$). Note how closely the Gaussian curve approximates the observed structure out to about 17° latitude.